INTERNATIONAL JOURNAL OF
NUMERICAL ANALYSIS AND MODELING
Volume 5, Number 4, Pages 543–569



# AN A PRIORI ERROR ANALYSIS OF OPERATOR UPSCALING FOR THE ACOUSTIC WAVE EQUATION

TETYANA VDOVINA AND SUSAN E. MINKOFF

**Abstract.** In many earth science problems, the scales of interest range from centimeters to kilometers. Computer power and time limitations prevent inclusion of all the fine-scale features in most models. However, upscaling methods allow creation of physically realistic and computationally feasible models. Instead of solving the problem completely on the fine scale, upscaling methods produce a coarse-scale solution that includes some of the fine-scale detail. Operator-based upscaling applied to the pressure/acceleration formulation of the acoustic wave equation solves the problem via decomposition of the solution into coarse and subgrid pieces. To capture local fine-scale information, small subgrid problems are solved independently in each coarse block. Then these local subgrid solutions are included in the definition of the coarse problem. In this paper, accuracy of the upscaled solution is determined via a detailed finite element analysis of the continuous-in-time and fully-discrete two-scale numerical schemes. We use lowest-order Raviart-Thomas mixed finite element approximation spaces on both the coarse and fine scales. Energy techniques show that in the $L^2$ norm the upscaled acceleration converges linearly on the coarse scale, and pressure (which is not upscaled in this implementation) converges linearly on the fine scale. The fully discrete scheme is also shown to be second-order in time. Three numerical experiments confirm the theoretical rate of convergence results.

**Key Words.** upscaling, convergence analysis, acoustic wave propagation, multiscale methods, error estimates.

## 1. Introduction

Data required for deep crustal seismic studies, time-lapse seismology, detailed near-surface environmental cleanup applications, and other modern-day earth-science problems can easily run into the terabyte range or beyond. Further, depending on the questions which need to be addressed in a particular study, the data may span a range of scales from centimeters to kilometers. Over the past few decades computational scientists and geoscientists have contributed to the development of various methods aimed at obtaining accurate and cost-effective solutions to these modeling problems. Finite-difference methods have long been accepted as an easy-to-implement and relatively accurate way to solve the discrete wave equation [14], [27], [28], [33]. While finite element methods for solving the wave equation have been proposed, they have not been as widely embraced in the geoscience modeling

Received by the editors May 9, 2007.
2000 *Mathematics Subject Classification.* 35L05, 86-08, 65M12, 65M15, 86A15.

community. These methods are better able to handle complex domain geometries, but they are more difficult to implement than finite-difference methods [28]. (For examples of finite element approaches to solving the wave equation, see [6], [7], [15], [16], [21], [22], [24], [25].)

Large-scale acoustic and elastic wave propagation in two and three dimensions has become computationally feasible in large part due to the successful implementation of data parallel algorithms (see [29] and works cited therein). In spatial (or data) parallelism, each processor has ownership of a subset of the total domain. The processor is responsible for allocating ghost cells at the boundaries of its subdomain, for updating the finite-difference solution over its portion of the domain (including along the ghost cells), and for communicating the boundary solution data to its immediate neighbors.

As an alternative to data parallelism (which includes all the collected data in the modeling but parcels the data out to different processors to reduce the computational load), techniques have emerged which attempt to either (1) determine the most important bits of data to incorporate in the model [34], (2) determine effective or homogenized input *parameters* for solving a coarser-scale problem [8], [11], [13], [23], or (3) approximate the *solution* via a subgrid upscaling procedure [1], [4], [12], [19].

In an earlier paper by Vdovina et al. [32], the authors presented the first extension of operator-based upscaling (originally developed for elliptic flow problems) to the acoustic wave equation. The key idea in operator upscaling is to solve the problem via a two-scale decomposition of the solution [4]. At the first stage, the problem is solved for the fine-scale (subgrid) unknowns defined locally within each coarse block. The method makes use of homogeneous Neumann boundary conditions between coarse blocks (in the first step) which allow for localization of the subgrid problems. At the second stage, we use the subgrid solutions to determine a new coarse-grid operator defined on the global domain. While the method was originally developed in the context of mixed finite elements, in practice the computationally intensive part of the algorithm (subgrid solve) is accomplished via finite differences. (We exploit the connection between lowest-order mixed finite elements and cell-centered finite differences [30], [32].) The method does not involve explicit averaging of the input parameters nor does it require scale separation or periodicity. We parallelize only the first stage of the algorithm (solving the much smaller coarse problem in serial). The main advantage of this upscaling approach over standard data parallelism is that there is no communication between processors since the subgrid problems decouple due to the boundary conditions used in the first stage of the process. We tested the numerical accuracy of the method on large domains with geophysically realistic input data typical of subsurface environments. Numerical experiments show that sub-wavelength scale heterogeneities were captured by the upscaled solution.

In a related paper, Korostyshevskaya and Minkoff [26] analyze the physical problem solved by the upscaling technique. What this analysis highlights is that the numerical upscaling process solves a constitutive equation similar in form to the original equation. The constitutive equation relates acceleration to the gradient of pressure. For the coarse (upscaled) problem, however, the parameter field (density) reduces to an averaged density along coarse block edges. Similarly, when analyzing the pressure equation, we find that the upscaled solution solves the original wave

equation at nodes internal to the coarse blocks but a modified equation at coarse block edges. Specifically, a cross-derivative (involving differentiation with respect to both $x$ and $y$ in 2D) enters the standard wave equation. This analysis not only simplifies the coding of the algorithm (for example by showing that the mass matrix in the upscaled equation is diagonal) but also illuminates the physical meaning of the upscaled solution.

Arbogast presents convergence theory for operator-based upscaling of elliptic problems in [2]. In Vdovina et al. [32], we outline a stability analysis based on the principle of energy conservation. In the current work, we use energy arguments together with this stability result to establish the first rigorous *a priori* error estimates for the continuous-in-time and fully-discrete solutions of the two-dimensional wave equation solved via operator upscaling. A number of standard finite element techniques for solving the acoustic wave equation have been shown to be convergent, including Galerkin [5], [17] and mixed finite element methods [16], [21]. Our work builds upon the literature (in particular, we apply the energy method to the acoustic wave equation as outlined in [16] and [21]). However, it differs from these works for the following reasons. First, we consider the pressure/acceleration formulation of the acoustic wave equation as opposed to the displacement formulation discussed in [21]. Secondly and more importantly, our discrete problem comes from the upscaling procedure. Thus the solution has a complicated two-scale structure. To account for the multiscale nature of the problem, we make use of operators (introduced in [2] by Arbogast) that map variational spaces onto the two-scale finite element subspaces. Using the approximation properties of these operators and confining our discussion of the method to lowest-order Raviart-Thomas mixed finite element spaces (RT0) for both coarse and subgrid problems, we show that pressure is approximated on the subgrid scale to order $h$ (fine-grid space step) in $L^2$ norm and acceleration is approximated on the coarse scale to order $H$ (coarse-grid space step). We have chosen to confine the theoretical discussion to the finite element spaces used in the implementation given in Vdovina et al. [32]. The results presented in this paper are the first rigorous estimates of operator upscaling for the wave equation, and they confirm the formal (local) order of accuracy results suggested by Korostyshevskaya and Minkoff [26].

In Sections 2 and 3, we introduce the model problem and summarize the upscaling algorithm mathematically. Section 4 explains our notation and contains background theory needed for the analysis which follows. In Section 5, we derive *a priori* error estimates for the continuous-in-time problem. Error estimates for the fully-discrete problem are given in Section 6. Finally, Section 7 contains three numerical tests that validate our theoretical results.

## 2. Model Problem and Weak Formulation

The following equation provides a classical formulation of the acoustic wave propagation problem:

$$\frac{1}{k(x,y)}\frac{\partial^2 p(t,x,y)}{\partial t^2} - \nabla\cdot\left(\frac{1}{\rho(x,y)}\nabla p(t,x,y)\right) = f(t,x,y), \tag{1}$$

where $p$ is pressure, $k(x,y)$ is bulk modulus, $\rho(x,y)$ is density, and $f$ is the source of acoustic energy.

In this work, we consider the pressure-acceleration formulation of the acoustic wave equation derived from the continuity equation and Newton's law. We assume that density $\rho$ is constant and denote velocity by $\mathbf{v}$. Then Newton's law becomes:

$$\frac{\partial \mathbf{v}(t,x,y)}{\partial t} = \mathbf{F} = -\nabla p(t,x,y), \tag{2}$$

where the force $\mathbf{F}$ is due to variations in pressure. The continuity equation relates the pressure drop to the divergence of velocity [9]:

$$-\frac{\partial p(t,x,y)}{\partial t} = k(x,y)\nabla \cdot \mathbf{v}(t,x,y). \tag{3}$$

If we differentiate this equation with respect to time and use the fact that in a constant-density medium $k(x,y) = c^2(x,y)$, then

$$-\frac{\partial^2 p(t,x,y)}{\partial t^2} = c^2(x,y)\nabla \cdot \left(\frac{\partial \mathbf{v}(t,x,y)}{\partial t}\right), \tag{4}$$

where $c(x,y)$ is the sound velocity. Introducing acceleration $\mathbf{u}$ as the time-derivative of velocity, we arrive at the pressure-acceleration formulation of the wave equation:

$$\mathbf{u}(t,x,y) = -\nabla p(t,x,y), \tag{5}$$

$$\frac{1}{c^2(x,y)}\frac{\partial^2 p(t,x,y)}{\partial t^2} + \nabla \cdot \mathbf{u}(t,x,y) = f(t,x,y). \tag{6}$$

Notice that equation (1) can be interpreted as an equation for potential $\phi$ defined by the time integral of pressure:

$$\phi(t,x,y) = \int_{-\infty}^{t} p(\tau,x,y)\, d\tau. \tag{7}$$

The velocity field is then determined from Newton's law:

$$\frac{\partial \mathbf{v}(t,x,y)}{\partial t} = -\nabla p(t,x,y) = -\nabla\left(\frac{\partial \phi(t,x,y)}{\partial t}\right) = -\frac{\partial}{\partial t}\nabla\phi(t,x,y). \tag{8}$$

Integration with respect to time gives velocity as the negative gradient of the pressure potential. Using the same continuity equation (3) to relate the pressure potential and velocity field, we obtain the potential-velocity formulation:

$$\mathbf{v}(t,x,y) = -\nabla\phi(t,x,y), \tag{9}$$

$$\frac{1}{c^2(x,y)}\frac{\partial^2 \phi(t,x,y)}{\partial t^2} + \nabla \cdot \mathbf{v}(t,x,y) = f(t,x,y). \tag{10}$$

Mathematically formulations (5)–(6) and (9)–(10) are equivalent. While the formulation involving the pressure potential leads to a clear physical interpretation of the results given later in this paper into potential and kinetic energy, we were motivated to examine the pressure-acceleration formulation instead because the latter involves measurable quantities which would be recorded by seismometers in real fields.

In general, the upscaling algorithm can accommodate any set of boundary and initial conditions. To simplify the presentation of the method, we consider the following conditions:

$$\mathbf{u} \cdot \boldsymbol{\nu} = 0 \quad \text{on } \Gamma, \tag{11}$$

$$p(0,x,y) = p_0, \qquad \frac{\partial p(0,x,y)}{\partial t} = p_1, \tag{12}$$

where $\boldsymbol{\nu}$ is the unit outward normal to the boundary $\Gamma$.

Let $\mathbf{V} = \mathbf{H}_0(\mathrm{div};\Omega)$ be the set of vector functions in $(L^2(\Omega))^2$ such that $\nabla\cdot\mathbf{v} \in L^2(\Omega)$ and $\mathbf{u}\cdot\boldsymbol{\nu} = 0$ on $\Gamma$. If we multiply equations (5)–(6) by $\mathbf{v}\in\mathbf{V}$ and $w\in L^2(\Omega)$, respectively, and integrate over $\Omega$, we obtain the variational formulation of our problem:

For $t \geq 0$ find $\mathbf{u}(t)\in\mathbf{V}$ and $p(t)\in L^2(\Omega)$ such that

$$(\mathbf{u}(0),\mathbf{v}) = (\mathbf{u}_0,\mathbf{v}), \tag{13}$$

$$(p(0),w) = (p_0,w), \tag{14}$$

$$(p_t(0),w) = (p_1,w), \tag{15}$$

$$(\mathbf{u}(t),\mathbf{v}) - (p(t),\nabla\cdot\mathbf{v}) = 0 \quad \text{for } t>0, \tag{16}$$

$$\left(\frac{1}{c^2}\frac{\partial^2 p(t)}{\partial t^2},w\right) + (\nabla\cdot\mathbf{u}(t),w) = (f(t),w) \quad \text{for } t>0 \tag{17}$$

for all $\mathbf{v}\in\mathbf{V}$ and $w\in L^2(\Omega)$. Equation (13) is an auxiliary condition which is derived from (5) and the initial conditions for pressure.

## 3. Operator-based Upscaling

The objective in operator-based upscaling is to construct a coarse-grid solution that incorporates some of the local fine-scale information without requiring solution of the full fine-scale problem. The method is based on decomposing the unknowns into coarse and subgrid pieces. To define this decomposition, we introduce a two-scale computational grid and construct the coarse acceleration space $\mathbf{V}_H \subset \mathbf{H}_0(\mathrm{div};\Omega)$ over the coarse mesh. The subgrid space $\delta\mathbf{V}_h \subset \mathbf{H}_0(\mathrm{div};E_c)$ is defined for each coarse element $E_c$. We localize the subgrid spaces by imposing homogeneous Neumann boundary conditions on each coarse block (see [32] for a discussion of the local boundary conditions). The two-scale acceleration space is given by a direct sum of the coarse and subgrid spaces:

$$\mathbf{V}_{H,h} = \mathbf{V}_H \oplus \delta\mathbf{V}_h. \tag{18}$$

Both spaces consist of linear functions of the form $(\alpha_1 x+\beta_1, \alpha_2 y+\beta_2)$ with nodes on the edges of the cells (see Figure 1).

Although we are able to upscale both pressure and acceleration, in prior related work [26] and [32] we chose not to upscale pressure. Upscaling pressure requires cumbersome basis functions and a more complicated algorithm (see [32] for a discussion of pressure upscaling). If required, a projection of pressure onto the coarse grid can be computed. Our analysis here applies to the implementation described in [32]. We use the full fine-scale pressure space that consists of piecewise discontinuous functions with nodes at the centers of the fine cells (see Figure 1). With this definition, computation of the pressure unknowns on the fine grid is performed locally inside each coarse element.

Using decomposition (18), we separate the acceleration unknowns into coarse and subgrid components $\mathbf{U} = \mathbf{U}_H + \delta\mathbf{U}$ and solve the problem in two stages. At the first stage, we solve a series of subgrid problems localized in each coarse element $E_c$. To obtain the variational form of these problems, we restrict to the subgrid test functions $\delta\mathbf{v}\in\delta\mathbf{V}_h$ and $w\in W_h$ in equations (16)–(17):

$$(\delta\mathbf{U}+\mathbf{U}_H,\delta\mathbf{v})_{E_c} - (P,\nabla\cdot\delta\mathbf{v})_{E_c} = 0, \tag{19}$$

$$\left(\frac{1}{c^2}\frac{\partial^2 P}{\partial t^2},w\right)_{E_c} + (\nabla\cdot(\delta\mathbf{U}+\mathbf{U}_H),w)_{E_c} = (f,w)_{E_c}. \tag{20}$$

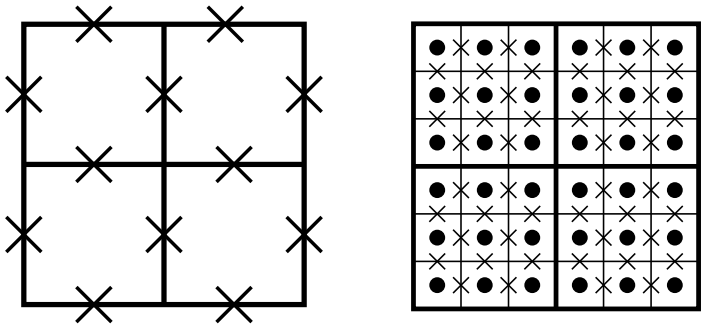

(a) (b)

FIGURE 1. (a) Coarse grid with $2 \times 2$ grid blocks. The large crosses represent the nodes in the coarse acceleration space $\mathbf{V}_H$. (b) Coarse grid with $2 \times 2$ coarse blocks and $3 \times 3$ subgrid blocks in each coarse block. The small crosses represent the nodes in the subgrid acceleration space $\delta\mathbf{V}_h(E_c)$. The dots represent the nodes in the pressure space $W_h$.

We use second-order finite differences to approximate the derivative with respect to time in equation (20). Subgrid acceleration $\delta\mathbf{U}$ is computed as a function of the (unknown) coarse solution $\mathbf{U}_H$. Since we do not upscale pressure, its computation is completed at the first stage. At the second stage, we use the subgrid solutions ($P$, $\delta\mathbf{U}$) and coarse test functions to define the problem on the coarse grid:

$$(\mathbf{U}_H + \delta\mathbf{U}, \mathbf{v})_\Omega - (P, \nabla \cdot \mathbf{v})_\Omega = 0 \tag{21}$$

for $\mathbf{v} \in \mathbf{V}_H$. The subgrid acceleration and pressure solutions allow local fine-scale information to be incorporated into the coarse problem. At this stage, the original global boundary conditions are used to solve the coarse problem. The algorithm repeats for the next time step.

At each time step of the upscaling algorithm we solve equations (19)–(20) and feed this subgrid solution into equation (21) which is then solved for the upscaled solution. One notes that $\mathbf{U}_H$ is unknown in equations (19)–(20). To circumvent this difficulty the traditional tack is to use numerical Green's functions (see [20, 3, 32]) which consists of breaking the subgrid problem into a set of simple subproblems using a superposition of solutions. The disadvantage of the numerical Green's functions approach is that it is computationally expensive (involving several matrix-vector products).

Korostyshevskaya and Minkoff [26] showed that the coarse-grid linear system reduces to an explicit difference equation in terms of pressure only, provided that fine-grid quadrature rules are used to approximate the inner products in equation (21). (Note that to make use of measured sound velocity and density in the acoustic wave equation, the implementation of the algorithm had always used fine grid quadrature to approximate the inner products so no added expense is incurred here.) Since the coarse problem is independent of subgrid acceleration, we were able to futher simplify the implementation of the method by eliminating subgrid acceleration altogether from the pressure equation. We solve the subgrid problems by replacing acceleration with the augmented solution. In the thesis by Vdovina

[31] she shows that the augmented acceleration solution (given by the sum of the coarse and subgrid components) reduces to the subgrid solution from the influence of the physical source at nodes internal to coarse blocks. At nodes located on coarse block edges, the augmented solution depends on the coarse component of acceleration only. Therefore, the complete subgrid acceleration solution is no longer required by the algorithm. The only component that is needed to solve the pressure equation or compute the augmented solution is the component of the solution that represents the influence of the physical source.

The modified algorithm can be summarized as follows:

(1) *For each time level:*
   i: Loop over all the coarse blocks to obtain the subgrid solutions from the physical source $f$ using a staggered finite-difference scheme.
   ii: Solve the coarse-grid problem for the coefficients in the finite element representation of coarse acceleration using an explicit difference equation.
   iii: Assemble the augmented solution using the component of the subgrid solutions from the physical source and coarse coefficients.

| number of processors | Finite-difference code | Original code | Modified upscaling code number of fine blocks per coarse block | | |
|---|---|---|---|---|---|
| | $100 \times 100$ | $100 \times 100$ | $100 \times 100$ | $60 \times 60$ | $50 \times 50$ |
| 1 | 29.43 | 67.01 | 29.69 | 29.92 | 30.31 |
| 2 | – | 34.20 | 15.46 | 15.35 | 15.61 |
| 4 | – | 17.19 | 7.63 | 7.97 | 8.59 |
| 6 | – | 11.57 | 5.23 | 5.62 | 5.88 |
| 8 | – | 10.69 | 4.37 | 5.12 | 7.52 |
| 12 | – | 7.39 | 3.07 | 3.82 | 3.97 |

TABLE 1. Observed time (in seconds) taken by the full finite-difference code (column 2), the original upscaling code described in [32] (column 3), and the modified upscaling code (columns 4–6) (time-step loop) for different numbers of processors and different groupings of fine grid blocks. Twenty time steps were taken in these experiments. The fine numerical grid contains $3600 \times 3600$ grid blocks.

Table 1 gives timing results for different sizes of coarse blocks and different numbers of processors for a domain discretized into $3600 \times 3600$ fine grid blocks. Columns 2, 3, and 4–6 of the table compare timings for a standard (non-upscaled) finite-difference solution of the wave equation, the original upscaling algorithm described in [32], and the modified upscaling algorithm described here respectively. We can see from columns 3 and 4 of Table 1 that the modified upscaling algorithm is more than two times faster than the algorithm described in [32]. In fact, even when run on a single processor, the modified upscaling code is quite comparable to a standard finite difference solution of the wave equation. When the problem is solved on 12 processors and upscaled to $100 \times 100$ coarse grid blocks, the upscaling algorithm is 10 times faster than straight finite-differences. (See [31] for the detailed discussion of the parallel performance of the modified algorithm.)

## 4. Notation and background theory

The $L^2$ inner product

$$(u, v) = \int_\Omega uv \, d\Omega \tag{22}$$

induces a norm which we denote by $||\cdot||_{L^2}$. In addition to the $L^2$ space norm, we introduce the following time-space norms:

$$\|u\|_{L^2(0,T;L^2(\Omega))} = \|u\|_{L^2(L^2)} = \left( \int_0^T \|u\|^2_{L^2(\Omega)} \, dt \right)^{\frac{1}{2}}, \tag{23}$$

$$\|u\|_{L^\infty(0,T;L^2(\Omega))} = \|u\|_{L^\infty(L^2)} = \max_{0 \le t \le T} \|u\|_{L^2(\Omega)}. \tag{24}$$

We derive the error estimates by showing that the numerical solution $(P, \mathbf{U})$ is close to a projection of the true solution $(p, \mathbf{u})$ onto the two-scale finite element spaces. Let $\mathcal{P}_h$ be the $L^2$ projection onto the pressure space $W_h$ such that

$$(\mathcal{P}_h \phi, w) = (\phi, w) \ \text{ for all } \phi \in L^2, \ \ w \in W_h. \tag{25}$$

In addition, if $\phi \in L^2 \cap H^l(\Omega)$, we have [10]

$$\|\mathcal{P}_h \phi - \phi\|_s \le C h^{j-s} \|\phi\|_j \ \text{ for } 0 \le s \le l, \ \ 0 \le j \le l, \tag{26}$$

where $l$ is associated with the degree of the approximating polynomial. Arbogast in [2] constructed an operator $\pi_{H,h}$ from $\mathbf{V} \cap \mathbf{H}^1$ onto the two-scale acceleration space $\mathbf{V}_{H,h}$ such that

$$\nabla \cdot \pi_{H,h} \mathbf{v} = \mathcal{P}_h \nabla \cdot \mathbf{v} \ \text{ for any } \mathbf{v} \in \mathbf{V} \cap \mathbf{H}^1 \tag{27}$$

and

$$\|\mathbf{v} - \pi_{H,h} \mathbf{v}\|_0 \le \|\mathbf{v}\|_m H^m, \ \ 0 \le m \le M, \tag{28}$$

where $M$ is the approximation order of the coarse acceleration space $\mathbf{V}_H$. To obtain an error estimate for the continuous-in-time problem, we use the following formulation of Gronwall's lemma [21]:

**Lemma 1.** *If $y(t) \ge 0$ satisfies $y_t \le k y(t) + h(t)$ for $0 \le t \le \tau$, where $k \ge 0$ is a constant and $h(t) \ge 0$, $h \in L^1(0, \tau)$, then*

$$y(t) \le e^{k\tau} \left[ y(0) + \int_0^\tau h(s) ds \right] \tag{29}$$

*for all $t \in [0, \tau]$.*

As in [16], [21], we use the "inverse inequality" to analyze the approximation properties of the fully-discrete problem:

**Lemma 2.** *Let $\rho(\mathcal{T})$ be the radius of a circle inscribed into element $\mathcal{T}$ of the partition of the grid, and let $h$ denote the maximum diameter. If there exists a constant $\nu > 0$ such that $\rho(\mathcal{T}) \ge \nu h$ for any element $\mathcal{T}$ in the partition of the grid, then*

$$\|\nabla \cdot \boldsymbol{\phi}\|_{L^2} \le K h^{-1} \|\boldsymbol{\phi}\|_{L^2}, \tag{30}$$

*where $K$ is independent of $h$ and $\boldsymbol{\phi} \in H(div; \mathcal{T})$.*

We refer the reader to [10], [18] for the proof of this result.

## 5. Continuous-in-time estimates

Our goal in this paper is to investigate the convergence properties of the operator-based upscaling algorithm. The algorithm produces a solution on the coarse grid. Therefore, coarse equation (21) is the most obvious candidate for analysis. However, in order to take into account subgrid acceleration and pressure defined on the fine grid, we use the approach followed by Arbogast [2] for elliptic problems. We will study the augmented two-scale problem:

Find $\mathbf{U}(t) \in \mathbf{V}_{H,h} = \mathbf{V}_H \oplus \delta\mathbf{V}$ and $P(t) \in W_h$ such that

$$(\mathbf{U}(0), \mathbf{v}) = (\pi_{H,h}\mathbf{u}_0, \mathbf{v}), \tag{31}$$

$$(P(0), w) = (p_0, w), \tag{32}$$

$$(P_t(0), w) = (p_1, w), \tag{33}$$

$$(\mathbf{U}, \mathbf{v}) - (P, \nabla \cdot \mathbf{v}) = 0 \quad \text{for } t > 0, \tag{34}$$

$$\left(\frac{1}{c^2}\frac{\partial^2 P}{\partial t^2}, w\right) + (\nabla \cdot \mathbf{U}, w) = (f(t), w) \quad \text{for } t > 0 \tag{35}$$

for all $\mathbf{v} \in \mathbf{V}_{H,h}$, $w \in W_h$. Although we do not solve this problem directly, we can easily construct the augmented acceleration solution from the coarse and subgrid solutions

$$\mathbf{U} = \mathbf{U}_H + \delta\mathbf{U}_h.$$

This post-processing step requires very little computational effort since it would be performed after completion of the time step loop, and at that point both the coarse and subgrid solutions are available from the upscaling process. In the theorem below, we derive an *a priori* error estimate for the continuous-in-time two-scale finite element scheme given in (31)–(35). We show that pressure and acceleration converge linearly on the fine and coarse scales, respectively, provided that RT0 mixed finite element spaces are used on both scales.

**Theorem 1.** *For $0 \le t \le T$ let $(p(t), \mathbf{u}(t))$ be the solution of problem (13)–(17) and $(P(t), \mathbf{U}(t))$ be the solution of problem (31)–(35). If $\mathbf{u} \in L^\infty(0,T;\mathbf{L}^2(\Omega))$, $\mathbf{u}_t \in L^2(0,T;\mathbf{H}^1(\Omega))$, $\mathbf{u}(0) \in \mathbf{H}^1(\Omega)$, $p_t \in L^\infty(0,T;L^2(\Omega))$, $p_{tt} \in L^2(0,T;H^1(\Omega))$, and $p_t(0) \in H^1(\Omega)$, then there exists a constant $K$ independent of $h$ and $H$ such that*

$$\begin{aligned} \left\| \frac{1}{c}(p_t - P_t) \right\|_{L^\infty(L^2)} &+ \|\mathbf{u} - \mathbf{U}\|_{L^\infty(L^2)} \\ &\le K\left(h\|p_{tt}\|_{L^2(H^1)} + H\|\mathbf{u}_t\|_{L^2(H^1)}\right). \end{aligned} \tag{36}$$

*Proof.* We consider the difference between the approximate solutions from the upscaling algorithm and solutions of equations (13)–(17). We add and subtract $\mathcal{P}_h p_t$ and $\pi_{H,h}\mathbf{u}$ and use the triangle inequality:

$$\begin{aligned} \left\| \frac{1}{c}(p_t - P_t) \right\|_{L^\infty(L^2)} &+ \|\mathbf{u} - \mathbf{U}\|_{L^\infty(L^2)} \\ &\le \left\| \frac{1}{c}(p_t - \mathcal{P}_h p_t) \right\|_{L^\infty(L^2)} + \|\mathbf{u} - \pi_{H,h}\mathbf{u}\|_{L^\infty(L^2)} \\ &+ \left\| \frac{1}{c}(P_t - \mathcal{P}_h p_t) \right\|_{L^\infty(L^2)} + \|\mathbf{U} - \pi_{H,h}\mathbf{u}\|_{L^\infty(L^2)}. \end{aligned} \tag{37}$$

First, we bound the difference between the true acceleration solution and its projection onto the finite element subspace:

$$\|\mathbf{u}-\pi_{H,h}\mathbf{u}\|_{L^2} = \|\mathbf{u}(0)-\pi_{H,h}\mathbf{u}(0)\|_{L^2} + \int_0^t \|\mathbf{u}_t-\pi_{H,h}\mathbf{u}_t\|_{L^2}\,d\tau \tag{38}$$
$$\leq \|\mathbf{u}(0)-\pi_{H,h}\mathbf{u}(0)\|_{L^2} + \int_0^T \|\mathbf{u}_t-\pi_{H,h}\mathbf{u}_t\|_{L^2}\,d\tau.$$

Using the Cauchy-Schwarz inequality on the integral term, we obtain:

$$\begin{aligned}\|\mathbf{u}-\pi_{H,h}\mathbf{u}\|_{L^2} &\leq \|\mathbf{u}(0)-\pi_{H,h}\mathbf{u}(0)\|_{L^2} \\ &+ \sqrt{T}\left(\int_0^T \|\mathbf{u}_t-\pi_{H,h}\mathbf{u}_t\|_{L^2}^2\,d\tau\right)^{1/2}.\end{aligned} \tag{39}$$

Then, taking the supremum over $t$ yields:

$$\begin{aligned}\|\mathbf{u}-\pi_{H,h}\mathbf{u}\|_{L^\infty(L^2)} &\leq \|\mathbf{u}(0)-\pi_{H,h}\mathbf{u}(0)\|_{L^2} + K\|\mathbf{u}_t-\pi_{H,h}\mathbf{u}_t\|_{L^2(L^2)} \\ &\leq KH\|\mathbf{u}_t\|_{L^2(H^1)},\end{aligned} \tag{40}$$

where the last inequality follows from approximation property (28) of operator $\pi_{H,h}$ and the fact that acceleration at time $t=0$ is a bounded function. Similarly, we can bound pressure by:

$$\left\|\frac{1}{c}(p_t-\mathcal{P}_h p_t)\right\|_{L^\infty(L^2)} \leq Kh\|p_{tt}\|_{L^2(H^1)}. \tag{41}$$

In the rest of the proof, we obtain a bound on the last two terms in (37) corresponding to the numerical approximation of pressure and acceleration. We begin with equations (16)–(17) and (34)–(35) and rewrite them in a form suitable for application of Gronwall's lemma. For notational convenience we let $\boldsymbol{\sigma} = \mathbf{U}-\pi_{H,h}\mathbf{u}$, $\xi = P-\mathcal{P}_h p$, $\boldsymbol{\eta} = \mathbf{u}-\pi_{H,h}\mathbf{u}$, and $\zeta = p-\mathcal{P}_h p$. If we subtract equations (16)–(17) from equations (34)–(35) and add and subtract $\mathcal{P}_h p_{tt}$ and $\pi_{H,h}\mathbf{u}$, we obtain:

$$(\boldsymbol{\sigma},\mathbf{v}) - (\xi,\nabla\cdot\mathbf{v}) = (\boldsymbol{\eta},\mathbf{v}) - (\zeta,\nabla\cdot\mathbf{v}), \tag{42}$$

$$\left(\frac{1}{c^2}\xi_{tt},w\right) + (\nabla\cdot\boldsymbol{\sigma},w) = \left(\frac{1}{c^2}\zeta_{tt},w\right) + (\nabla\cdot\boldsymbol{\eta},w). \tag{43}$$

We now differentiate (42) with respect to time:

$$(\boldsymbol{\sigma}_t,\mathbf{v}) - (\xi_t,\nabla\cdot\mathbf{v}) = (\boldsymbol{\eta}_t,\mathbf{v}) - (\zeta_t,\nabla\cdot\mathbf{v}). \tag{44}$$

Since $\boldsymbol{\sigma}$ belongs to $\mathbf{V}_{H,h}$ for each $t$, we can use $\mathbf{v}=\boldsymbol{\sigma}$ in equation (44). Also, since $\xi_t \in W_h$, we set $w=\xi_t$ in equation (43):

$$(\boldsymbol{\sigma}_t,\boldsymbol{\sigma}) - (\xi_t,\nabla\cdot\boldsymbol{\sigma}) = (\boldsymbol{\eta}_t,\boldsymbol{\sigma}) - (\zeta_t,\nabla\cdot\boldsymbol{\sigma}), \tag{45}$$

$$\left(\frac{1}{c^2}\xi_{tt},\xi_t\right) + (\nabla\cdot\boldsymbol{\sigma},\xi_t) = \left(\frac{1}{c^2}\zeta_{tt},\xi_t\right) + (\nabla\cdot\boldsymbol{\eta},\xi_t). \tag{46}$$

Adding these equations, we obtain:

$$\begin{aligned}\frac{1}{2}\frac{d}{dt}\left\|\frac{1}{c}\xi_t\right\|_{L^2}^2 &+ \frac{1}{2}\frac{d}{dt}\|\boldsymbol{\sigma}\|_{L^2}^2 \\ &= \left(\frac{1}{c^2}\zeta_{tt},\xi_t\right) + (\boldsymbol{\eta}_t,\boldsymbol{\sigma}) + (\nabla\cdot\boldsymbol{\eta},\xi_t) - (\zeta_t,\nabla\cdot\boldsymbol{\sigma}).\end{aligned} \tag{47}$$

Using definition (25) of the operator $\mathcal{P}_h$ and the fact that $\nabla \cdot \boldsymbol{\sigma} = \nabla \cdot (\mathbf{U} - \pi_{H,h}\mathbf{u})$ is in $W_h$, we show that the last term in equation (47) is equal to zero:

$$(\zeta_t, \nabla \cdot \boldsymbol{\sigma}) = (p_t - \mathcal{P}_h p_t, \nabla \cdot \boldsymbol{\sigma}) = 0. \tag{48}$$

Similarly, definitions (25) and (27) imply that

$$\begin{aligned} (\nabla \cdot \boldsymbol{\eta}, \xi_t) &= (\nabla \cdot \mathbf{u}, \xi_t) - (\nabla \cdot \pi_{H,h}\mathbf{u}, \xi_t) \\ &= (\nabla \cdot \mathbf{u}, \xi_t) - (\mathcal{P}_h \nabla \cdot \mathbf{u}, \xi_t) = 0, \end{aligned} \tag{49}$$

since $\mathcal{P}_h \nabla \cdot \mathbf{u}$, $\xi_t \in W_h$ and $\nabla \cdot \mathbf{u} \in L^2$. Using (48), (49), and the Cauchy-Schwarz inequality on the right-hand side of (47), we obtain:

$$\frac{1}{2}\frac{d}{dt}\left\|\frac{1}{c}\xi_t\right\|_{L^2}^2 + \frac{1}{2}\frac{d}{dt}\|\boldsymbol{\sigma}\|_{L^2}^2 \leq \left\|\frac{1}{c}\xi_t\right\|_{L^2}\left\|\frac{1}{c}\zeta_{tt}\right\|_{L^2} + \|\boldsymbol{\sigma}\|_{L^2}\|\boldsymbol{\eta}_t\|_{L^2}. \tag{50}$$

The algebraic inequality $2ab \leq a^2 + b^2$ can then be applied to the right-hand side of (50) to yield:

$$\begin{aligned} \frac{d}{dt}\left(\left\|\frac{1}{c}\xi_t\right\|_{L^2}^2 + \|\boldsymbol{\sigma}\|_{L^2}^2\right) &\leq \left\|\frac{1}{c}\xi_t\right\|_{L^2}^2 + \|\boldsymbol{\sigma}\|_{L^2}^2 \\ &+ \left\|\frac{1}{c}\zeta_{tt}\right\|_{L^2}^2 + \|\boldsymbol{\eta}_t\|_{L^2}^2. \end{aligned} \tag{51}$$

Applying Gronwall's lemma to the last inequality, we see that:

$$\begin{aligned} \left\|\frac{1}{c}\xi_t\right\|_{L^2}^2 + \|\boldsymbol{\sigma}\|_{L^2}^2 &\leq e^t\left(\left\|\frac{1}{c}\xi_t(0)\right\|_{L^2}^2 + \|\boldsymbol{\sigma}(0)\|_{L^2}^2\right) \\ &+ e^t\int_0^t\left(\left\|\frac{1}{c}\zeta_{tt}\right\|_{L^2}^2 + \|\boldsymbol{\eta}_t\|_{L^2}^2\right)d\tau. \end{aligned} \tag{52}$$

Initial conditions (13), (15), (31), and (33) imply that

$$\left\|\frac{1}{c}\xi_t(0)\right\|_{L^2}^2 + \|\boldsymbol{\sigma}(0)\|_{L^2}^2 = 0. \tag{53}$$

Taking the supremum over all $t$ in (52) gives:

$$\begin{aligned} \left\|\frac{1}{c}\xi_t\right\|_{L^\infty(L^2)}^2 + \|\boldsymbol{\sigma}\|_{L^\infty(L^2)}^2 &\leq K\left(\left\|\frac{1}{c}\zeta_{tt}\right\|_{L^2(L^2)}^2 + \|\boldsymbol{\eta}_t\|_{L^2(L^2)}^2\right) \\ &\leq K\left(h^2\left\|\frac{1}{c}p_{tt}\right\|_{L^2(H^1)}^2 + H^2\|\mathbf{u}_t\|_{L^2(H^1)}^2\right), \end{aligned} \tag{54}$$

where the last inequality follows from the approximation properties (26) and (28) and the constant $K$ includes an upper bound for $e^t$. Taking the square root of both sides of equation (54) and using it in the right-hand side of (37) together with bounds (40) and (41), we obtain the estimate of the theorem. □

## 6. Fully-discrete estimates

In this section, our goal is to analyze the approximation properties of the fully-discrete two-scale finite element problem. First, we discretize the derivative with respect to time using explicit second-order finite differences and introduce the fully-discrete problem. Then, we state the stability condition and use it to obtain *a priori* error estimates for the fully-discrete problem.

We begin by introducing the following notation for the discrete time derivatives:

$$D_t^2\phi^n = \frac{\phi^{n+1} - 2\phi^n + \phi^{n-1}}{(\Delta t)^2}, \tag{55}$$

$$D_t\phi^{n+\frac{1}{2}} = \frac{\phi^{n+1} - \phi^n}{\Delta t}, \tag{56}$$

where $\Delta t$ is the time step, $\phi^n$ denotes $\phi(t^n)$ for $t_n = n\Delta t$, and $t_N = T$. Setting $\phi^{n+\frac{1}{2}} = (\phi^n + \phi^{n+1})/2$, we obtain the following relation between the discrete time derivatives:

$$D_t^2\phi^n = \frac{D_t\phi^{n+\frac{1}{2}} - D_t\phi^{n-\frac{1}{2}}}{\Delta t} \quad . \tag{57}$$

We use this notation to formulate the fully-discrete two-scale finite element scheme: Find $(P^n, \mathbf{U}^n)$ in $W_h \times \mathbf{V}_{H,h}$ such that:

$$\left(\mathbf{U}^0, \mathbf{v}\right) = \left(\pi_{H,h}\mathbf{u}_0, \mathbf{v}\right), \tag{58}$$

$$\left(P^0, w\right) = \left(p_0, w\right), \tag{59}$$

$$\left(\frac{2}{\Delta t c^2}\frac{P^1 - P^0}{\Delta t}, w\right) + \left(\nabla\cdot\mathbf{U}^0, w\right) = \left(f^0 + \frac{2}{\Delta t c^2}p_1, w\right), \tag{60}$$

$$\left(\mathbf{U}^n, \mathbf{v}\right) - \left(P^n, \nabla\cdot\mathbf{v}\right) = 0, \tag{61}$$

$$\left(\frac{1}{c^2}D_t^2P^n, w\right) + \left(\nabla\cdot\mathbf{U}^n, w\right) = \left(f^n, w\right) \tag{62}$$

for $n$ from 1 to $N$ and all $w \in W_h$ and $\mathbf{v} \in \mathbf{V}_{H,h}$. In order to derive initial condition (60), we consider equation (62) at time level $n = 0$ :

$$\left(\frac{1}{c^2}\frac{P^1 - 2P^0 + P^{-1}}{(\Delta t)^2}, w\right) + \left(\nabla\cdot\mathbf{U}^0, w\right) = \left(f^0, w\right). \tag{63}$$

For this equation to be well-defined, we have to specify quantity $P^{-1}$. The appropriate value for $P^{-1}$ arises naturally in the proof of the theorem below (see Appendix A for details) and is defined in such a way that

$$\frac{P^1 - P^{-1}}{(\Delta t)^2} = \frac{2}{\Delta t}p_1. \tag{64}$$

Using relation (64) in (63), we obtain initial condition (60). In [32], we discuss the stability of problem (58)–(62) and derive the following condition using energy conservation:

**Lemma 3.** *The discrete problem (58)–(62) is stable if* $\Delta t < \dfrac{2h}{Kc_0}$ *for some constant* $K$ *independent of* $h$, $H$, *and* $\Delta t$. *That is, the temporal iterates*

$$\left(1 - \frac{K^2(\Delta t)^2c_0^2}{4h^2}\right)\|D_tP^n\|_{L^2}^2 + \|U^n\|_{L^2}^2 \tag{65}$$

*are bounded above by the initial data for all* $n$.

In the theorem below, we show that if the stability condition is satisfied, then the two-scale fully-discrete scheme (58)–(62) approximates pressure and acceleration to first order on the fine and coarse scales, respectively. The scheme is second-order in time, and the error estimates are obtained in the $l^\infty(L^2)$ norm.

**Theorem 2.** *For $0 \le t \le T$ let $(p(t), \mathbf{u}(t))$ be the solution of problem (13)–(17) and $(P^n, \mathbf{U}^n)$ be the solution of problem (58)–(62). If $\mathbf{u} \in L^\infty(\mathbf{H}^1(\Omega))$, $p, \dfrac{\partial p}{\partial t}, \dfrac{\partial^3 p}{\partial t^3}, \dfrac{\partial^4 p}{\partial t^4} \in L^\infty(H^1(\Omega))$, then there exists a constant $K$ independent of $h$, $H$, and $\Delta t$ such that if $\Delta t < 2h/Kc_0$, then*

$$\left\| \frac{1}{c}(p-P) \right\|_{l^\infty(L^2)} + \|\mathbf{u}-\mathbf{U}\|_{l^\infty(L^2)} \le K \left( h \|p\|_{L^\infty(H^1)} + H \|\mathbf{u}\|_{L^\infty(H^1)} \right.$$

$$\left. + h \left\| \frac{\partial p}{\partial t} \right\|_{L^\infty(H^1)} + (\Delta t)^2 \left\| \frac{\partial^3 p}{\partial t^3} \right\|_{L^\infty(H^1)} + (\Delta t)^2 \left\| \frac{\partial^4 p}{\partial t^4} \right\|_{L^\infty(H^1)} \right). \tag{66}$$

*Proof.* As before, we begin by considering the difference between the solutions of approximate equations (58)–(62) and solutions of equations (13)–(17). We then add and subtract $\mathcal{P}_h p$ and $\pi_{H,h}\mathbf{u}$ and use the triangle inequality:

$$\begin{aligned} \left\| \frac{1}{c}(p-P) \right\|_{l^\infty(L^2)} &+ \|\mathbf{u}-\mathbf{U}\|_{l^\infty(L^2)} \\ &\le \left\| \frac{1}{c}(p-\mathcal{P}_h p) \right\|_{l^\infty(L^2)} + \|\mathbf{u}-\pi_{H,h}\mathbf{u}\|_{l^\infty(L^2)} \\ &+ \left\| \frac{1}{c}(P-\mathcal{P}_h p) \right\|_{l^\infty(L^2)} + \|\mathbf{U}-\pi_{H,h}\mathbf{u}\|_{l^\infty(L^2)}. \end{aligned} \tag{67}$$

The proof consists of two parts. In Part I, we bound the first two terms on the right-hand side of (67). These terms correspond to the difference between the true pressure and acceleration solutions and their projections onto the finite element subspaces. Therefore, we can directly apply approximation properties (26) and (28) of operators $\mathcal{P}_h$ and $\pi_{H,h}$ to obtain the bound. In Part II, our goal is to estimate the last two terms of (67) corresponding to the numerical approximation of pressure and acceleration. These terms do not allow the direct application of the approximation inequalities, since they do not involve the true solution. However, a careful choice of test functions will reintroduce the true solution into these terms.

**Part I.** In this part of the proof, we show that the difference between the true solutions $p$ and $\mathbf{u}$ and their projections onto the finite element spaces can be bounded as follows:

$$\begin{aligned} \left\| \frac{1}{c}(p-\mathcal{P}_h p) \right\|_{l^\infty(L^2)} &+ \|\mathbf{u}-\pi_{H,h}\mathbf{u}\|_{l^\infty(L^2)} \\ &\le K \left( h \|p\|_{L^\infty(H^1)} + H \|\mathbf{u}\|_{L^\infty(H^1)} \right). \end{aligned} \tag{68}$$

To obtain this bound, notice that

$$\begin{aligned} \left\| \frac{1}{c}(p^n-\mathcal{P}_h p^n) \right\|_{L^2} &+ \|\mathbf{u}^n-\pi_{H,h}\mathbf{u}^n\|_{L^2} \\ &\le \left\| \frac{1}{c}(p-\mathcal{P}_h p) \right\|_{L^\infty(L^2)} + \|\mathbf{u}-\pi_{H,h}\mathbf{u}\|_{L^\infty(L^2)} \\ &\le K \left( h \|p\|_{L^\infty(H^1)} + H \|\mathbf{u}\|_{L^\infty(H^1)} \right), \end{aligned} \tag{69}$$

where the last inequality follows from approximation properties (26) and (28). Taking the supremum over the time levels in (69) leads to inequality (68).

**Part II.** In this part of the proof, we obtain the following bound on the difference between approximate pressure and acceleration and the projections $\mathcal{P}_h p$ and $\pi_{H,h}\mathbf{u}$:

$$\begin{aligned}\left\|\frac{1}{c}\left(P-\mathcal{P}_h p\right)\right\|_{l^\infty(L^2)} &+ \left\|\mathbf{U}-\pi_{H,h}\mathbf{u}\right\|_{l^\infty(L^2)} \\ &\leq K\left(H\left\|\mathbf{u}\right\|_{L^\infty(H^1)}+h\left\|\frac{\partial p}{\partial t}\right\|_{L^\infty(H^1)}\right. \\ &+ \left.(\Delta t)^2\left\|\frac{\partial^3 p}{\partial t^3}\right\|_{L^\infty(H^1)}+(\Delta t)^2\left\|\frac{\partial^4 p}{\partial t^4}\right\|_{L^\infty(H^1)}\right).\end{aligned} \tag{70}$$

As before, let $\boldsymbol{\sigma}^n = \mathbf{U}^n - \pi_{H,h}\mathbf{u}^n$, $\xi^n = P^n - \mathcal{P}_h p^n$, $\boldsymbol{\eta}^n = \mathbf{u}^n - \pi_{H,h}\mathbf{u}^n$, and $\zeta^n = p^n - \mathcal{P}_h p^n$. First, we consider the acceleration equations (61) and (16) at time level $n+1$. Subtracting these equations and using projection property (25), we obtain:

$$(\boldsymbol{\sigma}^{n+1},\mathbf{v})-(\xi^{n+1},\nabla\cdot\mathbf{v})=(\boldsymbol{\eta}^{n+1},\mathbf{v}) \quad \text{for } n\geq 0. \tag{71}$$

Similarly, if we subtract the pressure equations (62) and (17) and then add and subtract the discrete derivative of the true solution $p$ and its projection $\mathcal{P}_h p$ we get:

$$\begin{aligned}\left(\frac{1}{c^2}D_t^2\xi^n,w\right) &+ (\nabla\cdot\boldsymbol{\sigma}^n,w)=\left(\frac{1}{c^2}D_t^2\zeta^n,w\right) \\ &+ \left(\frac{1}{c^2}\left(\frac{\partial^2 p(t^n)}{\partial t^2}-D_t^2 p^n\right),w\right)+(\nabla\cdot\boldsymbol{\eta}^n,w) \quad \text{for } n\geq 1.\end{aligned} \tag{72}$$

From properties (25) and (27) of operators $\mathcal{P}_h$ and $\pi_{H,h}$, we obtain that $(\nabla\cdot\boldsymbol{\eta}^n,w)=0$ for all $n$.

To obtain a bound on $\|1/c\,(P-\mathcal{P}_h p)\|_{L^2}$ and $\|\mathbf{U}-\pi_{H,h}\mathbf{u}\|_{L^2}$, we have to introduce appropriate terms into equations (71) and (72). In the case of the acceleration equation, this can be done directly by suitable choice of test function $\mathbf{v}$. Equation (72), however, involves the second time derivative of pressure. We integrate equation (72) in the discrete sense with respect to time. We begin by using relation (57) for the time derivatives in (72):

$$\begin{aligned}\left(\frac{1}{c^2}\frac{D_t\xi^{n+\frac{1}{2}}-D_t\xi^{n-\frac{1}{2}}}{\Delta t},w\right) &+ (\nabla\cdot\boldsymbol{\sigma}^n,w) \\ &= \left(\frac{1}{c^2}\frac{D_t\zeta^{n+\frac{1}{2}}-D_t\zeta^{n-\frac{1}{2}}}{\Delta t},w\right)+(r^n,w),\end{aligned} \tag{73}$$

where $r^n$ is defined as follows:

$$r^n=\frac{1}{c^2}\left(\frac{\partial^2 p(t^n)}{\partial t^2}-D_t^2 p^n\right) \quad \text{for } n\geq 1. \tag{74}$$

Then, multiplying equation (73) by $\Delta t$ and summing over the time levels gives:

$$\begin{aligned}\left(\frac{1}{c^2}\left(D_t\xi^{n+\frac{1}{2}}-D_t\xi^{\frac{1}{2}}\right),w\right) &+ (\Delta t\sum_{i=1}^{n}\nabla\cdot\boldsymbol{\sigma}^i,w) \\ &= \left(\frac{1}{c^2}\left(D_t\zeta^{n+\frac{1}{2}}-D_t\zeta^{\frac{1}{2}}\right),w\right)+(\Delta t\sum_{i=1}^{n}r^i,w).\end{aligned} \tag{75}$$

At this point, we would like to use the initial conditions to simplify equation (75). Initial pressure appears in the first inner products on the left- and right-hand sides

of (75). In order to include initial acceleration into this equation, we introduce the following quantities:

$$\boldsymbol{\phi}^0 = \frac{\Delta t}{2}\boldsymbol{\sigma}^0, \quad \boldsymbol{\phi}^n = \boldsymbol{\phi}^0 + \Delta t \sum_{i=1}^{n} \boldsymbol{\sigma}^i. \tag{76}$$

Then, $\Delta t \sum_{i=1}^{n} \boldsymbol{\sigma}^i = \boldsymbol{\phi}^n - \boldsymbol{\phi}^0$ and equation (75) becomes:

$$\begin{aligned} \left(\frac{1}{c^2} D_t \xi^{n+\frac{1}{2}}, w\right) &+ (\nabla \cdot \boldsymbol{\phi}^n, w) = \left(\frac{1}{c^2}\left(D_t \zeta^{n+\frac{1}{2}} - D_t \zeta^{\frac{1}{2}}\right), w\right) \\ &+ \left(\frac{1}{c^2} D_t \xi^{\frac{1}{2}}, w\right) + (\nabla \cdot \boldsymbol{\phi}^0, w) + (\Delta t \sum_{i=1}^{n} r^i, w). \end{aligned} \tag{77}$$

Initial conditions (60) and (15) imply the following relation for the terms on the right-hand side of (77) (see Appendix A for details) :

$$\begin{aligned} \left(\frac{1}{c^2} D_t \xi^{\frac{1}{2}}, w\right) &+ (\nabla \cdot \boldsymbol{\phi}^0, w) - \left(\frac{1}{c^2} D_t \zeta^{\frac{1}{2}}, w\right) \\ &= -\frac{1}{2\Delta t c^2} \int_0^{\Delta t} (t - \Delta t)^2 \left(\frac{\partial^3 p(t)}{\partial t^3}, w\right) dt. \end{aligned} \tag{78}$$

This relation allows us to reduce (77) to

$$\left(\frac{1}{c^2} D_t \xi^{n+\frac{1}{2}}, w\right) + (\nabla \cdot \boldsymbol{\phi}^n, w) = \left(\frac{1}{c^2} D_t \zeta^{n+\frac{1}{2}}, w\right) + (R^n, w), \tag{79}$$

where

$$R^n = \Delta t \sum_{i=0}^{n} r^i, \tag{80}$$

$$r^0 = -\frac{1}{2(\Delta t)^2 c^2} \int_0^{\Delta t} (t - \Delta t)^2 \frac{\partial^3 p(t)}{\partial t^3} dt, \tag{81}$$

and $r^i$ is given by equation (74) for $i \geq 1$. Definition (56) of the time derivatives that appear in equation (79) suggests the following choice of test function $w = (\xi^{n+1} + \xi^n)/2 \in W_h$. Using this test function in (79), we obtain:

$$\begin{aligned} &\frac{1}{2\Delta t}\left(\left\|\frac{1}{c}\xi^{n+1}\right\|_{L^2}^2 - \left\|\frac{1}{c}\xi^{n}\right\|_{L^2}^2\right) + \left(\nabla \cdot \boldsymbol{\phi}^n, \frac{\xi^{n+1} + \xi^n}{2}\right) \\ &= \left(\frac{1}{c^2} D_t \zeta^{n+\frac{1}{2}}, \frac{\xi^{n+1} + \xi^n}{2}\right) + \left(R^n, \frac{\xi^{n+1} + \xi^n}{2}\right) \quad \text{for } n \geq 0. \end{aligned} \tag{82}$$

Since we have now introduced the term $\|1/c\,(P - \mathcal{P}_h p)\|_{L^2}$ into the pressure equation, we return to the acceleration equation (71). We notice from definition (76) of $\boldsymbol{\phi}^n$ that $\boldsymbol{\sigma}^{n+1} = (\boldsymbol{\phi}^{n+1} - \boldsymbol{\phi}^n)/\Delta t$. Using this fact together with test function $\mathbf{v} = (\boldsymbol{\phi}^{n+1} + \boldsymbol{\phi}^n)/2 \in \mathbf{V}_{H,h}$ in (71) leads to the following equation:

$$\begin{aligned} \frac{1}{2\Delta t}\left(\left\|\boldsymbol{\phi}^{n+1}\right\|_{L^2}^2 - \left\|\boldsymbol{\phi}^{n}\right\|_{L^2}^2\right) &- \left(\xi^{n+1}, \nabla \cdot \frac{\boldsymbol{\phi}^{n+1} + \boldsymbol{\phi}^n}{2}\right) \\ &= \left(\boldsymbol{\eta}^{n+1}, \frac{\boldsymbol{\phi}^{n+1} + \boldsymbol{\phi}^n}{2}\right) \quad \text{for } n \geq 0. \end{aligned} \tag{83}$$

We now add the pressure and acceleration equations (82) and (83) and multiply by $2\Delta t$ to obtain:

$$
\begin{aligned}
\left\|\frac{1}{c}\xi^{n+1}\right\|_{L^2}^2 &- \left\|\frac{1}{c}\xi^{n}\right\|_{L^2}^2 + \left\|\boldsymbol{\phi}^{n+1}\right\|_{L^2}^2 - \left\|\boldsymbol{\phi}^{n}\right\|_{L^2}^2 \\
&+ \Delta t[(\nabla\cdot\boldsymbol{\phi}^n,\xi^n) - (\xi^{n+1},\nabla\cdot\boldsymbol{\phi}^{n+1})] \\
&= \Delta t\left(\frac{1}{c^2}D_t\zeta^{n+\frac{1}{2}},\xi^{n+1}+\xi^n\right) \\
&+ \Delta t(R^n,\xi^{n+1}+\xi^n) + \Delta t(\boldsymbol{\eta}^{n+1},\boldsymbol{\phi}^{n+1}+\boldsymbol{\phi}^n).
\end{aligned} \tag{84}
$$

Notice that in addition to the terms we would like to bound, the left-hand side of (84) contains extra terms. Summing over time levels gives:

$$
\begin{aligned}
\left\|\frac{1}{c}\xi^{n+1}\right\|_{L^2}^2 &- \left\|\frac{1}{c}\xi^{0}\right\|_{L^2}^2 + \left\|\boldsymbol{\phi}^{n+1}\right\|_{L^2}^2 - \left\|\boldsymbol{\phi}^{0}\right\|_{L^2}^2 \\
&+ \Delta t[(\nabla\cdot\boldsymbol{\phi}^0,\xi^0) - (\xi^{n+1},\nabla\cdot\boldsymbol{\phi}^{n+1})] \\
&= \Delta t\sum_{i=0}^{n}\left(\frac{1}{c^2}D_t\zeta^{i+\frac{1}{2}},\xi^{i+1}+\xi^i\right) \\
&+ \Delta t\sum_{i=0}^{n}\left(R^i,\xi^{i+1}+\xi^i\right) + \Delta t\sum_{i=0}^{n}\left(\boldsymbol{\eta}^{i+1},\boldsymbol{\phi}^{i+1}+\boldsymbol{\phi}^i\right).
\end{aligned} \tag{85}
$$

The initial conditions imply that $\left\|\frac{1}{c}\xi^0\right\|_{L^2}$, $\left\|\boldsymbol{\phi}^0\right\|_{L^2}$, and $(\nabla\cdot\boldsymbol{\phi}^0,\xi^0)$ are zero. In order to eliminate the divergence term from the left-hand side of (85), we apply the Cauchy-Schwarz inequality, the inverse assumption (30), and an algebraic inequality to this term:

$$
\begin{aligned}
\Delta t(\xi^{n+1},\nabla\cdot\boldsymbol{\phi}^{n+1}) &\leq \Delta t\left\|\xi^{n+1}\right\|_{L^2}\left\|\nabla\cdot\boldsymbol{\phi}^{n+1}\right\|_{L^2} \\
&\leq \frac{K\Delta t}{h}\left\|\xi^{n+1}\right\|_{L^2}\left\|\boldsymbol{\phi}^{n+1}\right\|_{L^2} \\
&\leq \frac{K\Delta t c_0}{2h}\left(\left\|\frac{1}{c}\xi^{n+1}\right\|_{L^2}^2 + \left\|\boldsymbol{\phi}^{n+1}\right\|_{L^2}^2\right),
\end{aligned} \tag{86}
$$

where $c_0$ is an upper bound on the sound velocity and K includes constants from Lemmas 2 and 3. Choosing $h$ and $\Delta t$ so that $K\Delta t c_0/2h < 1$, we have that:

$$
\Delta t(\xi^{n+1},\nabla\cdot\boldsymbol{\phi}^{n+1}) < \left\|\frac{1}{c}\xi^{n+1}\right\|_{L^2}^2 + \left\|\boldsymbol{\phi}^{n+1}\right\|_{L^2}^2. \tag{87}
$$

Using inequality (87) in the left-hand side of (85) and the Cauchy-Schwarz inequality on the right-hand side, we obtain:

$$
\begin{aligned}
K\left(\left\|\frac{1}{c}\xi^{n+1}\right\|_{L^2}^2 \quad + \quad \left\|\boldsymbol{\phi}^{n+1}\right\|_{L^2}^2\right) & \\
\leq \quad \Delta t\sum_{i=0}^{n}\left\|\frac{1}{c^2}D_t\zeta^{i+\frac{1}{2}}\right\|_{L^2}\left(\left\|\xi^{i+1}\right\|_{L^2}+\left\|\xi^{i}\right\|_{L^2}\right) & \\
+ \quad \Delta t\sum_{i=0}^{n}\left\|R^{i}\right\|_{L^2}\left(\left\|\xi^{i+1}\right\|_{L^2}+\left\|\xi^{i}\right\|_{L^2}\right) & \\
+ \quad \Delta t\sum_{i=0}^{n}\left\|\boldsymbol{\eta}^{i+1}\right\|_{L^2}\left(\left\|\boldsymbol{\phi}^{i+1}\right\|_{L^2}+\left\|\boldsymbol{\phi}^{i}\right\|_{L^2}\right), &
\end{aligned}
\tag{88}
$$

where $K$ is some constant less than 1. Multiplying (88) by $1/K$ and using the fact that $\left\|\xi^{i}\right\|_{L^2} \leq \|\xi\|_{l^\infty(L^2)}$ and $\left\|\boldsymbol{\phi}^{i}\right\|_{L^2} \leq \|\boldsymbol{\phi}\|_{l^\infty(L^2)}$, we obtain:

$$
\begin{aligned}
\left\|\frac{1}{c}\xi^{n+1}\right\|_{L^2}^2 \quad + \quad \left\|\boldsymbol{\phi}^{n+1}\right\|_{L^2}^2 & \\
\leq \quad K\Delta t\left\|\frac{1}{c}\xi\right\|_{l^\infty(L^2)}\left(\sum_{i=0}^{N}\left\|\frac{1}{c^2}D_t\zeta^{i+\frac{1}{2}}\right\|_{L^2}+\sum_{i=0}^{N}\left\|R^{i}\right\|_{L^2}\right) & \\
+ \quad K\Delta t\left\|\boldsymbol{\phi}\right\|_{l^\infty(L^2)}\sum_{i=0}^{N}\left\|\boldsymbol{\eta}^{i+1}\right\|_{L^2}, &
\end{aligned}
\tag{89}
$$

where we have renamed the appropriate constant $K$ again. Applying the algebraic inequalities $ab \leq 1/4a^2 + b^2$ and $(a+b)^2 \leq 2(a^2+b^2)$ to the right-hand side of the last inequality gives:

$$
\begin{aligned}
\left\|\frac{1}{c}\xi^{n+1}\right\|_{L^2}^2 \quad + \quad \left\|\boldsymbol{\phi}^{n+1}\right\|_{L^2}^2 & \\
\leq \quad \frac{1}{4}\left\|\frac{1}{c}\xi\right\|_{l^\infty(L^2)}^2 + K\left(\Delta t\sum_{i=0}^{N}\left\|\frac{1}{c^2}D_t\zeta^{i+\frac{1}{2}}\right\|_{L^2}\right)^2 & \\
+ \quad K\left(\Delta t\sum_{i=0}^{N}\left\|R^{i}\right\|_{L^2}\right)^2 & \\
+ \quad \frac{1}{4}\left\|\boldsymbol{\phi}\right\|_{l^\infty(L^2)}^2 + K\left(\Delta t\sum_{i=0}^{N}\left\|\boldsymbol{\eta}^{i+1}\right\|_{L^2}\right)^2. &
\end{aligned}
\tag{90}
$$

Taking the supremum over time levels on the left-hand side of the last inequality, we have that

$$
\begin{aligned}
\left\|\frac{1}{c}\xi\right\|_{l^\infty(L^2)}^2 \quad + \quad \left\|\boldsymbol{\phi}\right\|_{l^\infty(L^2)}^2 \leq K\left(\Delta t\sum_{i=0}^{N}\left\|\frac{1}{c^2}D_t\zeta^{i+\frac{1}{2}}\right\|_{L^2}\right)^2 & \\
+ \quad K\left(\Delta t\sum_{i=0}^{N}\left\|R^{i}\right\|_{L^2}\right)^2 + K\left(\Delta t\sum_{i=0}^{N}\left\|\boldsymbol{\eta}^{i+1}\right\|_{L^2}\right)^2. &
\end{aligned}
\tag{91}
$$

To complete part II of the proof, we need to bound each term on the right-hand side of (91). We begin with the first term on the right-hand side of (91) and derive

the following auxiliary estimate:

$$\begin{aligned}
\left\| \frac{1}{c^2} D_t \zeta^{i+\frac{1}{2}} \right\|_{L^2}^2 &= \left\| \frac{1}{c^2} D_t \left( p^{i+\frac{1}{2}} - \mathcal{P}_h p^{i+\frac{1}{2}} \right) \right\|_{L^2}^2 \\
&= \frac{1}{(\Delta t)^2} \left\| \frac{1}{c^2} \left[ (p(t_{i+1}) - \mathcal{P}_h p(t_{i+1})) - (p(t_i) - \mathcal{P}_h p(t_i)) \right] \right\|_{L^2}^2 \\
&= \frac{1}{(\Delta t)^2} \left\| \frac{1}{c^2} \int_{t_i}^{t_{i+1}} \frac{\partial}{\partial t} \left( p(t) - \mathcal{P}_h p(t) \right) \, dt \right\|_{L^2}^2 \qquad (92) \\
&= \frac{1}{(\Delta t)^2} \int_\Omega \left[ \frac{1}{c^2} \int_{t_i}^{t_{i+1}} \frac{\partial}{\partial t} \left( p(t) - \mathcal{P}_h p(t) \right) \, dt \right]^2 d\Omega.
\end{aligned}$$

The Cauchy-Schwarz inequality gives that:

$$\begin{aligned}
\left\| \frac{1}{c^2} D_t \zeta^{i+\frac{1}{2}} \right\|_{L^2}^2 &\leq \frac{K}{(\Delta t)^2} \int_\Omega \int_{t_i}^{t_{i+1}} dt \int_{t_i}^{t_{i+1}} \left[ \frac{\partial}{\partial t} \left( p(t) - \mathcal{P}_h p(t) \right) \right]^2 dt \, d\Omega \\
&\leq \frac{K}{(\Delta t)^2} \int_\Omega \Delta t \int_{t_i}^{t_{i+1}} \left[ \frac{\partial}{\partial t} \left( p(t) - \mathcal{P}_h p(t) \right) \right]^2 dt \, d\Omega \\
&\leq \frac{K}{\Delta t} \int_{t_i}^{t_{i+1}} \left\| \frac{\partial}{\partial t} \left( p(t) - \mathcal{P}_h p(t) \right) \right\|_{L^2}^2 dt \qquad (93) \\
&\leq \frac{K}{\Delta t} \left\| \frac{\partial}{\partial t} \left( p(t) - \mathcal{P}_h p(t) \right) \right\|_{L^\infty(L^2)}^2 \int_{t_i}^{t_{i+1}} dt \\
&\leq K h^2 \left\| \frac{\partial p(t)}{\partial t} \right\|_{L^\infty(H^1)}^2,
\end{aligned}$$

where the last inequality follows from the approximation property (26) of the operator $\mathcal{P}_h$ and the constant $K$ includes an upper bound on $1/c^2$. We take square roots of both sides of inequality (93) and use it to bound the first term on the right-hand side of (91):

$$\begin{aligned}
\Delta t \sum_{i=0}^{N} \left\| \frac{1}{c^2} D_t \zeta^{i+\frac{1}{2}} \right\|_{L^2} &\leq \Delta t \sum_{i=0}^{N} K h \left\| \frac{\partial p(t)}{\partial t} \right\|_{L^\infty(H^1)} \qquad (94) \\
&\leq K T h \left\| \frac{\partial p(t)}{\partial t} \right\|_{L^\infty(H^1)}.
\end{aligned}$$

Next, we bound the last term of (91) using approximation property (28) of $\pi_{H,h}$ :

$$\begin{aligned}
\Delta t \sum_{i=0}^{N} \left\| \boldsymbol{\eta}^{i+1} \right\|_{L^2} &= \Delta t \sum_{i=0}^{N} \left\| \mathbf{u}((i+1)\Delta t) - \pi_{H,h} \mathbf{u}((i+1)\Delta t) \right\|_{L^2} \\
&\leq \Delta t H \sum_{i=0}^{N} \left\| \mathbf{u}((i+1)\Delta t) \right\|_{H^1} \leq N \Delta t H \left\| \mathbf{u} \right\|_{L^\infty(H^1)} \qquad (95) \\
&\leq T H \left\| \mathbf{u} \right\|_{L^\infty(H^1)}.
\end{aligned}$$

Finally, we turn our attention to the second term on the right-hand side of (91): From definition (80) of $R^i$, we have that:

$$\begin{aligned}(96)\qquad \Delta t\sum_{i=0}^{N}\left\|R^i\right\|_{L^2} &\le \Delta t\sum_{i=0}^{N}\left[\Delta t\sum_{j=1}^{i}\left\|r^j\right\|_{L^2}+\Delta t\left\|r^0\right\|_{L^2}\right]\\ &\le (\Delta t)^2\sum_{i=0}^{N}\left[\sum_{j=1}^{i}\left\|r^j\right\|_{L^2}+\left\|\frac{1}{2(\Delta t)^2c^2}\int_0^{\Delta t}(t-\Delta t)^2\frac{\partial^3 p(t)}{\partial t^3}dt\right\|_{L^2}\right],\end{aligned}$$

where the integral term comes from definition (81) of $r^0$. We bound each term in (96) separately starting with $r^j$. We recall the definition of $r^j$ (equation (74)):

$$(97)\quad r^j=\frac{1}{c^2}\left(\frac{\partial^2 p}{\partial t^2}(t_j)-D_t^2p^j\right)=\frac{1}{c^2}\left(\frac{\partial^2 p}{\partial t^2}(t_j)-\frac{p^{j+1}-2p^j+p^{j-1}}{(\Delta t)^2}\right).$$

Using Taylor expansions of $p^{j-1}$ and $p^{j+1}$ around the point $t_j$, we obtain:

$$\begin{aligned}p^{j+1}+p^{j-1} &= 2p^j+\frac{\partial^2 p}{\partial t^2}(t_j)(\Delta t)^2+\frac{1}{6}\left[\int_{t_j}^{t_{j+1}}(t_j+\Delta t-t)^3\frac{\partial^4 p(t)}{\partial t^4}dt\right.\\ &- \left.\int_{t_{j-1}}^{t_j}(t_j-\Delta t-t)^3\frac{\partial^4 p(t)}{\partial t^4}dt\right] \qquad (98)\\ &= 2p^j+\frac{\partial^2 p}{\partial t^2}(t_j)(\Delta t)^2+\frac{1}{6}\int_{-\Delta t}^{\Delta t}(\Delta t-|t|)^3\frac{\partial^4 p(t_j+t)}{\partial t^4}dt,\end{aligned}$$

where we have combined the integrals via the change of variables $t=t_j+t$. Substituting (98) into (97), we reduce $r^j$ to a single integral term:

$$(99)\qquad r^j=-\frac{1}{6c^2(\Delta t)^2}\int_{-\Delta t}^{\Delta t}(\Delta t-|t|)^3\frac{\partial^4 p(t_j+t)}{\partial t^4}\,dt.$$

To obtain a bound for $\left\|r^j\right\|_{L^2}$ we first use the fact that the maximum of $(\Delta t-|t|)^3$ on $(-\Delta t,\Delta t)$ is achieved at $t=0$. The maximum value is $(\Delta t)^3$. Then

$$\begin{aligned}\left\|r^j\right\|_{L^2}^2 &\le \frac{K}{(\Delta t)^4}\int_\Omega\left[\max_{-\Delta t<\xi<\Delta t}(\Delta t-|\xi|)^3\int_{-\Delta t}^{\Delta t}\frac{\partial^4 p(t_j+t)}{\partial t^4}dt\right]^2 d\Omega\\ &\le K(\Delta t)^2\int_\Omega\left[\int_{-\Delta t}^{\Delta t}\frac{\partial^4 p(t_j+t)}{\partial t^4}dt\right]^2 d\Omega, \qquad (100)\end{aligned}$$

where $K$ includes an upper bound on $1/(6c^2)$. Then, we make the change of variables $t_j+t=t$, apply the Cauchy-Schwarz inequality to the integral with respect to time,

and interchange the integration with respect to the time and space variables:

$$\begin{aligned}
\left\|r^j\right\|_{L^2}^2 &\leq K(\Delta t)^2 \int_\Omega \left[\int_{t_j-\Delta t}^{t_j+\Delta t} \frac{\partial^4 p(t)}{\partial t^4}\, dt\right]^2 d\Omega \\
&\leq K(\Delta t)^2 \int_\Omega 2\Delta t \int_{t_j-\Delta t}^{t_j+\Delta t} \left(\frac{\partial^4 p(t)}{\partial t^4}\right)^2 dt\, d\Omega \qquad (101)\\
&\leq K(\Delta t)^3 \int_{t_j-\Delta t}^{t_j+\Delta t} \int_\Omega \left(\frac{\partial^4 p(t)}{\partial t^4}\right)^2 d\Omega\, dt \\
&\leq K(\Delta t)^3 \int_{t_j-\Delta t}^{t_j+\Delta t} \left\|\frac{\partial^4 p(t)}{\partial t^4}\right\|_{L^2}^2 dt \leq K(\Delta t)^4 \left\|\frac{\partial^4 p(t)}{\partial t^4}\right\|_{L^\infty(L^2)}^2 .
\end{aligned}$$

In a similar way we can bound the second term on the right-hand side of (96):

$$\left\|\frac{1}{2(\Delta t)^2 c^2}\int_0^{\Delta t}(t-\Delta t)^2 \frac{\partial^3 p(t)}{\partial t^3} dt\right\|_{L^2}^2 \leq K(\Delta t)^2 \left\|\frac{\partial^3 p(t)}{\partial t^3}\right\|_{L^\infty(L^2)}^2 . \qquad (102)$$

Taking square roots on both sides of estimates (101) and (102) and using the results in (96), we obtain the bound on $\left\|R^i\right\|_{L^2}$:

$$\begin{aligned}
&\Delta t \sum_{i=0}^{N} \left\|R^i\right\|_{L^2} \\
&\leq K(\Delta t)^2 \sum_{i=0}^{N} \left[\sum_{j=0}^{i} (\Delta t)^2 \left\|\frac{\partial^4 p(t)}{\partial t^4}\right\|_{L^\infty(L^2)} + \Delta t \left\|\frac{\partial^3 p(t)}{\partial t^3}\right\|_{L^\infty(L^2)}\right] \qquad (103)\\
&\leq K(\Delta t)^2 \left(N^2(\Delta t^2) \left\|\frac{\partial^4 p(t)}{\partial t^4}\right\|_{L^\infty(L^2)} + N\Delta t \left\|\frac{\partial^3 p(t)}{\partial t^3}\right\|_{L^\infty(L^2)}\right) \\
&\leq K(\Delta t)^2 \left(\left\|\frac{\partial^4 p(t)}{\partial t^4}\right\|_{L^\infty(L^2)} + \left\|\frac{\partial^3 p(t)}{\partial t^3}\right\|_{L^\infty(L^2)}\right),
\end{aligned}$$

where we have renamed the constant $K$ in the last inequality to include $T^2 = N^2(\Delta t)^2$. Finally, we obtain (70) by combining the bounds (94), (95), and (103) on the right-hand side of (91). Statement (66) follows immediately from inequalities (68) and (70) used in the right-hand side of (67). □

## 7. Numerical Experiments

We note that the theory discussed in the previous sections is valid so long as the sound velocity is slowly varying and bounded. In real subsurface environments, variation in parameters would occur on a number of scales. On the smallest scale the rock material would likely be well mixed and vary fairly smoothly in older sedimentary regions. However, on a larger scale suitable for numerical computation one might expect discontinuities in measured sound velocity from one grid point to the next in the computational domain. In this paper we verify the convergence theory by running numerical experiments where the medium is homogeneous, and the source function is chosen to produce a known analytic solution (in other words, true norm errors can be calculated as a test of rate of convergence).

The utility of the upscaling algorithm of course arises from applying it to heterogeneous earth models, and these more realistic cases was explored extensively

in the earlier paper by Vdovina et al. [32]. Specifically in that paper we describe three distinct upscaling examples involving heterogeneous earth models. In the first experiment the sound velocity includes two velocity values which alternate in a periodic checkerboard. In the second experiment the velocity field is a finely layered medium typical of subsurface regions such as the Gulf of Mexico. The final experiment uses a velocity field which is a single realization from a stochastic von Karman distribution of a two-component material mixture. The latter experiment is representative of the type of detail possible in deep crustal seismic studies where such long wavelengths are required to reach the depth of investigation that all small-scale information must be described statistically rather than deterministically. All of these experiments contain features typical of select subsurface regions and all contain heterogeneities which are subwavelength-scale (i.e., the heterogeneities vary on a scale smaller than a single coarse grid block). For example, in the case of the thinly layered medium, each layer is two fine grid blocks wide. However, the domain is discretized so that ten fine blocks are grouped into one coarse block. Hence the scale of the layers is considerably smaller than the width of the coarse blocks. Nonetheless, the augmented upscaled solution compares quite favorably with the full fine scale finite difference solution. The finely-layered structural discontinuities are clearly evident in the augmented upscaled solution.

In this section, we validate the theory just described by presenting three numerical experiments. Our primary aim is to numerically illustrate the convergence rate predicted by Theorem 2. In Experiment 1, we assume each coarse block contains only one fine grid block. In this case, the pressure solution will be a function of coarse-grid acceleration only (subgrid acceleration will be zero), and, therefore, the algorithm should converge at the rate expected of standard RT0 mixed finite elements without upscaling. In Experiment 2, the number of coarse grid blocks is fixed at 100 in both the horizontal and vertical directions. The number of fine grid blocks per coarse block does change in this experiment, however. Our goal in this experiment is to demonstrate that pressure converges linearly on the fine scale. Finally, in Experiment 3, the number of fine blocks is fixed (6400 in each of the two directions). In this case, the number of coarse blocks (and hence the number of fine blocks per coarse block) varies. We demonstrate that acceleration converges linearly on the coarse scale.

In all the experiments, we consider a square domain of size $\Omega = 100$ m $\times 100$ m with a homogeneous sound velocity of 1000 m/s. We used a source function of the following form:

$$\begin{aligned} f(t,x,y) &= \frac{2}{c^2}\left(1-\cos\left(\frac{2\pi x}{100}\right)\right)\left(1-\cos\left(\frac{2\pi y}{100}\right)\right) \\ &- 4\pi^2 t(t-\Delta t)\left(\cos\left(\frac{2\pi x}{100}\right)+\cos\left(\frac{2\pi y}{100}\right)-2\cos\left(\frac{2\pi x}{100}\right)\cos\left(\frac{2\pi y}{100}\right)\right). \end{aligned}$$

This source function was chosen in order to produce the closed-form pressure solution:

$$p(t,x,y) = t(t-\Delta t)\left(1-\cos\left(\frac{2\pi x}{100}\right)\right)\left(1-\cos\left(\frac{2\pi y}{100}\right)\right).$$

Similarly, since acceleration is the negative gradient of pressure, we can calculate an analytic expression for the acceleration solution. We chose the time and space discretizations so that the stability condition is satisfied, and the number of grid

points per wavelength is sufficient to eliminate dispersion effects. (See [32] for an extensive discussion of stability and dispersion as well as guidelines for the choice of time step size in practice.)

Tables 2–4 summarize the convergence studies performed in Experiments 1–3. In Tables 2–3, the first two columns show the number of grid blocks in the fine and coarse discretizations, respectively. Columns three and four give the time step size and total number of time steps. Finally, the last two columns contain the relative pressure and acceleration errors (difference between upscaled and analytic solutions). Table 4 shows the same information, although in this experiment the fine grid is fixed so the time step size is also fixed (as determined by the CFL condition which comes from the fine grid [32]). In Experiment 1, the number of grid blocks in the fine and coarse grids are the same. In each row of the table a different test is performed. Specifically, we halve the spatial grid spacing and time step size and consider wave propagation for a total of $3.53 \times 10^{-2}$ s. (Note that we have to double the number of time iterations in each subtest in order to obtain results for comparison at the same final time.) Since we used the RT0 mixed finite element method, we expect to see linear convergence for both pressure and acceleration. Table 2 shows that, as expected, both variables converge linearly.

| Number of fine blocks | Number of coarse blocks | Time step (s) | Number of time steps | $\frac{\|\|P-p\|\|_0}{\|\|p\|\|_1}$ | $\frac{\|\|\mathbf{U}-\mathbf{u}\|\|_0}{\|\|\mathbf{u}\|\|_1}$ |
|---|---|---|---|---|---|
| $16 \times 16$ | $16 \times 16$ | $4.41 \cdot 10^{-3}$ | 100 | $2.46 \cdot 10^{-2}$ | $2.63 \cdot 10^{-2}$ |
| $32 \times 32$ | $32 \times 32$ | $2.21 \cdot 10^{-3}$ | 200 | $9.75 \cdot 10^{-3}$ | $1.14 \cdot 10^{-2}$ |
| $64 \times 64$ | $64 \times 64$ | $1.10 \cdot 10^{-3}$ | 400 | $4.26 \cdot 10^{-3}$ | $5.30 \cdot 10^{-3}$ |
| $128 \times 128$ | $128 \times 128$ | $5.52 \cdot 10^{-4}$ | 800 | $1.98 \cdot 10^{-3}$ | $2.54 \cdot 10^{-3}$ |
| $256 \times 256$ | $256 \times 256$ | $2.76 \cdot 10^{-4}$ | 1600 | $9.51 \cdot 10^{-4}$ | $1.24 \cdot 10^{-3}$ |
| $512 \times 512$ | $512 \times 512$ | $1.38 \cdot 10^{-4}$ | 3200 | $4.66 \cdot 10^{-4}$ | $6.17 \cdot 10^{-4}$ |

TABLE 2. Pressure and acceleration relative errors for Experiment 1.

In Experiment 2, we see that the upscaling algorithm preserves the linear convergence of pressure on the fine scale. We fix the coarse-grid discretization and halve the subgrid spatial and time step sizes in each subtest, increasing the number of time iterations. Table 3 shows that, as expected, the acceleration error remains constant in all the subtests since the coarse grid is fixed, and the pressure solution exhibits a linear rate of convergence.

| Number of fine blocks | Number of coarse blocks | Time step (s) | Number of time steps | $\frac{\|\|P-p\|\|_0}{\|\|p\|\|_1}$ | $\frac{\|\|\mathbf{U}-\mathbf{u}\|\|_0}{\|\|\mathbf{u}\|\|_1}$ |
|---|---|---|---|---|---|
| $400 \times 400$ | $100 \times 100$ | $1.77 \cdot 10^{-4}$ | 200 | $5.48 \cdot 10^{-3}$ | $1.28 \cdot 10^{-2}$ |
| $800 \times 800$ | $100 \times 100$ | $8.83 \cdot 10^{-5}$ | 400 | $2.75 \cdot 10^{-3}$ | $1.11 \cdot 10^{-2}$ |
| $1600 \times 1600$ | $100 \times 100$ | $4.42 \cdot 10^{-5}$ | 800 | $1.40 \cdot 10^{-3}$ | $1.06 \cdot 10^{-2}$ |
| $3200 \times 3200$ | $100 \times 100$ | $2.21 \cdot 10^{-5}$ | 1600 | $7.27 \cdot 10^{-4}$ | $1.05 \cdot 10^{-2}$ |
| $6400 \times 6400$ | $100 \times 100$ | $1.10 \cdot 10^{-5}$ | 3200 | $3.97 \cdot 10^{-4}$ | $1.04 \cdot 10^{-2}$ |

TABLE 3. Pressure and acceleration relative errors for Experiment 2.

In Experiment 3, our goal is to demonstrate that the upscaled acceleration converges linearly on the coarse grid. We fix the number of fine grid blocks in the domain and reduce the coarse-grid step size by a factor of two in each subtest. Since time step $\Delta t$ is determined from the sound velocity and fine step size only, we use the same $\Delta t = 1.104 \times 10^{-5}$ s for all the subtests. We ran the simulation for 3200 time steps. Table 4 shows that, as predicted by our theoretical results, acceleration converges linearly, while the pressure error remains constant.

| Number of fine blocks | Number of coarse blocks | $\frac{\|\|P-p\|\|_0}{\|\|p\|\|_1}$ | $\frac{\|\|\mathbf{U}-\mathbf{u}\|\|_0}{\|\|\mathbf{u}\|\|_1}$ |
|---|---|---|---|
| $6400 \times 6400$ | $100 \times 100$ | $3.97 \cdot 10^{-4}$ | $1.04 \cdot 10^{-2}$ |
| $6400 \times 6400$ | $200 \times 200$ | $3.50 \cdot 10^{-4}$ | $5.24 \cdot 10^{-3}$ |
| $6400 \times 6400$ | $400 \times 400$ | $3.41 \cdot 10^{-4}$ | $2.65 \cdot 10^{-3}$ |
| $6400 \times 6400$ | $800 \times 800$ | $3.39 \cdot 10^{-4}$ | $1.38 \cdot 10^{-3}$ |
| $6400 \times 6400$ | $1600 \times 1600$ | $3.39 \cdot 10^{-4}$ | $7.97 \cdot 10^{-4}$ |

TABLE 4. Pressure and acceleration relative errors for Experiment 3. The number of time steps is 3200 with time step size $\Delta t = 1.104 \times 10^{-5}$ s.

## 8. Conclusion

Many geoscience problems involve data at a very fine scale or at multiple scales. Models which use this data will require large amounts of computer memory and time. One way to circumvent reliance on fine scale data is to employ upscaling methods. These methods formulate and solve a coarse-scale problem but incorporate some of the fine-scale information into the coarse solution. The accuracy of upscaling algorithms is usually difficult to determine due to the complicated multiscale structure of the resulting solution. One of the attractions of homogenization-based techniques has been that asymptotic theory allows calculation of errors. However, homogenization requires periodicity and scale-separation. Neither assumption is realistic for most geoscience applications.

Operator-based upscaling solves problems in two stages:

(1) Fine-scale information is captured within each coarse grid block at the subgrid stage;
(2) The fine-scale subgrid solution is incorporated into the coarse problem to be solved.

As with most upscaling methods, operator-based upscaling was originally developed and analyzed for elliptic pde's. In the paper by Vdovina et al. [32], we extended operator upscaling to hyperbolic problems. The method parallelizes nicely. In fact, the primary savings of the algorithm comes from the fact that there is no communication between coarse blocks at the (expensive) subgrid stage. Numerical examples indicate that the upscaled solution does capture sub-wavelength scale fluctuations in the coarse solution. In a second paper [26], Korostyshevskaya and Minkoff determined which physical problem is solved by operator upscaling applied to the acoustic wave equation. Specifically, within each coarse element, the pressure solution (which comes from a second-order finite-difference stencil equivalent to lowest-order mixed finite elements on the fine grid) is second-order accurate. Along

the coarse element edges, however, the upscaled solution solves a modified version of the wave equation. Thus formally the physical analysis indicated that we would lose one order of accuracy globally (linear convergence).

In summary, in prior work we have shown that operator-based upscaling applied to the acoustic wave equation produces an efficient and physically meaningful solution. In the current work, our goal was to rigorously investigate the global approximation properties of the upscaling algorithm via standard energy estimate techniques and projection operators. We derived global *a priori* error estimates for the continuous-in-time and fully-discrete two-scale numerical schemes that use RT0 approximation spaces on both the fine and coarse grids. Upscaled acceleration converges linearly on the coarse scale, and pressure converges linearly on the fine grid. The fully-discrete scheme is second order in time. The *a priori* error estimates agreed with our earlier physical intuition and were confirmed via numerical experiments.

## Appendix A

In this appendix, we show that if the initial condition for the discrete-in-time problem is given by

$$\left(\frac{2}{\Delta t c^2}\frac{P^1-P^0}{\Delta t},w\right)+\left(\nabla\cdot\mathbf{U}^0,w\right) = \left(f^0+\frac{2}{\Delta t c^2}p_1,w\right) \tag{A-1}$$

for $w\in W_h$, then

$$\begin{aligned}\left(\frac{1}{c^2}D_t\xi^{\frac{1}{2}},w\right) &+ (\nabla\cdot\boldsymbol{\phi}^0,w)-\left(\frac{1}{c^2}D_t\zeta^{\frac{1}{2}},w\right)\\ &= -\frac{1}{2\Delta t c^2}\int_0^{\Delta t}(t-\Delta t)^2\left(\frac{\partial^3 p(t)}{\partial t^3},w\right)dt.\end{aligned} \tag{A-2}$$

We recall that $\xi^{\frac{1}{2}}=P^{\frac{1}{2}}-\mathcal{P}_h p^{\frac{1}{2}}$, $\zeta^{\frac{1}{2}}=p^{\frac{1}{2}}-\mathcal{P}_h p^{\frac{1}{2}}$, and $\boldsymbol{\phi}^0=\frac{\Delta t}{2}\left(\mathbf{U}^0-\pi_{H,h}\mathbf{u}^0\right)$. Then, the left-hand side of equation (A-2) becomes

$$\begin{aligned}\left(\frac{1}{c^2}D_t\xi^{\frac{1}{2}},w\right) &+ (\nabla\cdot\boldsymbol{\phi}^0,w)-\left(\frac{1}{c^2}D_t\zeta^{\frac{1}{2}},w\right)\\ &= \left(\frac{1}{c^2}D_t\left(P^{\frac{1}{2}}-\mathcal{P}_h p^{\frac{1}{2}}\right),w\right)+\frac{\Delta t}{2}\left(\nabla\cdot\left(\mathbf{U}^0-\pi_{H,h}\mathbf{u}^0\right),w\right)\\ &- \left(\frac{1}{c^2}D_t\left(p^{\frac{1}{2}}-\mathcal{P}_h p^{\frac{1}{2}}\right),w\right)\\ &= \left(\frac{1}{c^2}\frac{P^1-P^0}{\Delta t},w\right)+\frac{\Delta t}{2}\left(\nabla\cdot\mathbf{U}^0,w\right)\\ &- \frac{\Delta t}{2}\left(\nabla\cdot\pi_{H,h}\mathbf{u}^0,w\right)-\left(\frac{1}{c^2}\frac{p^1-p^0}{\Delta t},w\right)\\ &= \left(\frac{1}{c^2}\frac{P^1-P^0}{\Delta t},w\right)+\frac{\Delta t}{2}\left(\nabla\cdot\mathbf{U}^0,w\right)\\ &- \frac{\Delta t}{2}\left(\nabla\cdot\mathbf{u}^0,w\right)-\frac{1}{c^2}\left(\frac{p(\Delta t)-p(0)}{\Delta t},w\right),\end{aligned} \tag{A-3}$$

where we use definitions (25) and (27) to show that $\left(\nabla \cdot \pi_{H,h}\mathbf{u}^0, w\right) = \left(\mathcal{P}_h \nabla \cdot \mathbf{u}^0, w\right)$ $= \left(\nabla \cdot \mathbf{u}^0, w\right)$. At time $t = 0$, solutions $p$ and $\mathbf{u}$ satisfy equation (17). Therefore,

$$-\frac{\Delta t}{2}\left(\nabla \cdot \mathbf{u}(0), w\right) = \frac{\Delta t}{2}\left(\frac{1}{c^2}\frac{\partial p^2(0)}{\partial t^2}, w\right) - \frac{\Delta t}{2}(f^0, w). \tag{A-4}$$

We substitute equation (A-4) into (A-3):

$$\begin{aligned}\left(\frac{1}{c^2}D_t\xi^{\frac{1}{2}}, w\right) &+ (\nabla \cdot \boldsymbol{\phi}^0, w) - \left(\frac{1}{c^2}D_t\zeta^{\frac{1}{2}}, w\right) \\ &= \left(\frac{1}{c^2}\frac{P^1 - P^0}{\Delta t}, w\right) + \frac{\Delta t}{2}\left(\nabla \cdot \mathbf{U}^0, w\right) \\ &+ \frac{\Delta t}{2}\left(\frac{1}{c^2}\frac{\partial p^2(0)}{\partial t^2}, w\right) - \frac{\Delta t}{2}(f^0, w) - \left(\frac{1}{c^2}\frac{p(\Delta t) - p(0)}{\Delta t}, w\right).\end{aligned} \tag{A-5}$$

We expand $p$ into a Taylor series around zero to obtain

$$\frac{\Delta t}{2}\frac{\partial p^2(0)}{\partial t^2} = \frac{p(\Delta t) - p(0)}{\Delta t} - p_t(0) - \frac{1}{2\Delta t}\int_0^{\Delta t}(\Delta t - t)^2\frac{\partial^3 p}{\partial t^3}dt \tag{A-6}$$

Substituting this expansion into equation (A-5) yields:

$$\begin{aligned}\left(\frac{1}{c^2}D_t\xi^{\frac{1}{2}}, w\right) &+ (\nabla \cdot \boldsymbol{\phi}^0, w) - \left(\frac{1}{c^2}D_t\zeta^{\frac{1}{2}}, w\right) \\ &= \left(\frac{1}{c^2}\frac{P^1 - P^0}{\Delta t}, w\right) + \frac{\Delta t}{2}\left(\nabla \cdot \mathbf{U}^0, w\right) - \frac{\Delta t}{2}(f^0, w) \\ &- \left(\frac{1}{c^2}p_t(0), w\right) - \frac{1}{2c^2\Delta t}\int_0^{\Delta t}(\Delta t - t)^2\left(\frac{\partial^3 p}{\partial t^3}, w\right)dt.\end{aligned} \tag{A-7}$$

Finally, initial condition (A-1) implies that

$$\begin{aligned}\left(\frac{1}{c^2}D_t\xi^{\frac{1}{2}}, w\right) &+ (\nabla \cdot \boldsymbol{\phi}^0, w) - \left(\frac{1}{c^2}D_t\zeta^{\frac{1}{2}}, w\right) \\ &= -\frac{1}{2c^2\Delta t}\int_0^{\Delta t}(\Delta t - t)^2\left(\frac{\partial^3 p}{\partial t^3}, w\right)dt.\end{aligned} \tag{A-8}$$

## Acknowledgments

We thank Bill Symes of Rice University for his help interpreting the experimental rate of convergence results. We are also grateful to Eleanor Jenkins of Clemson University for providing helpful supporting material from her paper. This research was performed with funding from the Collaborative Math-Geoscience Program at NSF (grant #EAR-0222181). The first author was also supported during the 2005–2006 academic year by a graduate student fellowship generously provided by NASA Goddard's Earth Sciences and Technology Center (GEST).

## References

[1] T. Arbogast. An overview of subgrid upscaling for elliptic problems in mixed form. In Z. Chen, R. Glowinski, and Kaitai Li, editors, *Current Trends in Scientific Computing*, pages 21–32. American Mathematical Society, Providence, RI, 2003.

[2] T. Arbogast. Analysis of a two-scale, locally conservative subgrid upscaling for elliptic problems. *SIAM Journal on Numerical Analysis*, 42:576–598, 2004.

[3] T. Arbogast and S. Bryant. A two-scale numerical subgrid technique for waterflood simulations. *SPE Journal*, 27:446–457, 2002.

[4] T. Arbogast, S. Minkoff, and P. Keenan. An operator-based approach to upscaling the pressure equation. In V. Burganos, G. Karatzas, A. Payatakes, C. Brebbia, W. Gray, and G. Pinder, editors, *Computational Methods in Water Resources XII*, pages 405–412. Computational Mechanics Publications, Southhampton, UK, 1998.

[5] G. Baker. Error estimates for finite element methods for second order hyperbolic equations. *SIAM Journal on Numerical Analysis*, 13:564–576, 1976.

[6] A. Bamberger, R. Glowinski, and Q. H. Tran. A domain decomposition method for the acoustic wave equation with discontinuous coefficients and grid change. *SIAM Journal on Numerical Analysis*, 34:603–639, 1997.

[7] E. Becache, P. Joly, and C. Tsogka. An analysis of new mixed finite elements for the approximation of wave propagation problems. *SIAM Journal on Numerical Analysis*, 37:1053–1084, 2000.

[8] A. Bensoussan, J. Lions, and G. Papanicolaou. *Asymptotic Analysis for Periodic Structure*. North Holland, New York, 1979.

[9] D. Braess. *Finite Elements: Theory, Fast Solvers, and Applications in Solid Mechanics*. Cambridge University Press, New York, 1997.

[10] F. Brezzi and M. Fortin. *Mixed and Hybrid Finite Element Methods*. Springer-Verlag, New York, 1991.

[11] Z. Chen. Large-scale averaging analysis of single phase flow in fractured reservoirs. *SIAM J. Appl. Math.*, 54:641–659, 1994.

[12] Z. Chen and T. Hou. A mixed multiscale finite element method for elliptic problems with oscillating coefficients. *Math. Comp.*, 72:541–576, 2002.

[13] M. Christie. Upscaling for reservoir simulation. *J. Pet. Tech.*, 48:1004–1010, 1996.

[14] G. Cohen. *Higher-Order Numerical Methods for Transient Wave Equations*. Springer-Verlag, New York, 2002.

[15] G. Cohen and S. Fauqueux. Mixed spectral finite elements for the linear elasticity system in unbound domains. *SIAM Journal on Scientific Computing*, 26:864–884, 2005.

[16] L.C. Cowsar, T.F. Dupont, and M. F. Wheeler. A priori estimates for mixed finite element approximations of second-order hyperbolic equations with absorbing boundary conditions. *SIAM Journal on Numerical Analysis*, 33:492–504, 1996.

[17] T. Dupont. L2 estimates for Galerkin methods for second order hyperbolic equations. *SIAM Journal on Numerical Analysis*, 10:880–889, 1973.

[18] H. Fujita, N. Saito, and T. Suzuku. *Operator Theory and Numerical Methods*. North Holland, New York, 2001.

[19] T. Hou and X. Wu. A multiscale finite element method for elliptic problems in composite materials and porous media. *Journal of Computational Physics*, 134:169–189, 1997.

[20] T. Hughes. Multiscale phenomena: Green's functions, the Dirichlet-to-Neumann formulation, subgrid scale models, bubbles and the origins of stabilized methods. *Comput. Methods Appl. Mech. Engrg.*, 127:387–401, 1995.

[21] E. Jenkins, B. Riviére, and M. F. Wheeler. A priori error estimates for mixed finite element approximations of the acoustic wave equation. *SIAM Journal on Numerical Analysis*, 40:1698–1715, 2002.

[22] P. Joly. *Variational Methods for Time-Dependent Wave Propagation Problems*, volume 31 of *Lecture Notes in Computational Science and Engineering*. Springer-Verlag, Berlin, 2003.

[23] P. King and J. Williams. Upscaling permeability: Mathematics of renormalization. *Transp. Porous Media*, 23:337–354, 1996.

[24] D. Komatitsch, S. Tsuboi, and J. Tromp. *The Spectral-Element Method in Seismology*, volume 157 of *Geophysical Monograph Series*. American Geophysical Union, 2005.

[25] D. Komatitsch, J.-P. Vilotte, R. Vai, J. Castillo-Covarrubias, and F. Sanchez-Sesma. The spectral-element method for elastic wave equations – application to 2-d and 3-d seismic problems. *International Journal for Numerical Methods in Engineering*, 45:1139–1664, 1999.

[26] O. Korostyshevskaya and S. Minkoff. A matrix analysis of operator-based upscaling for the wave equation. *SIAM Journal on Numerical Analysis*, 44:586–612, 2006.

[27] A. Levander. Fourth-order finite-difference P-SV seismograms. *Geophysics*, 53:1425–1436, 1988.

[28] K. Marfurt. Accuracy of finite-difference and finite-element modeling of the scalar and elastic wave equations. *Geophysics*, 49:553–549, 1984.

[29] S. Minkoff. Spatial parallelism of a 3d finite difference, velocity-stress elastic wave propagation code. *SIAM J. Scientific Computing*, 24:1–19, 2002.
[30] T. Russell and M. F. Wheeler. *The Mathematics of Reservoir Simulation*. SIAM, Philadelphia, 1983.
[31] T. Vdovina. *Operator Upscaling for the Wave Equation*. PhD thesis, University of Maryland Baltimore County, Baltimore, MD, 2006.
[32] T. Vdovina, S. Minkoff, and O. Korostyshevskaya. Operator upscaling for the acoustic wave equation. *SIAM Journal on Multiscale Modeling and Simulation*, 4:1305–1338, 2005.
[33] J. Virieux. P-SV wave propagation in heterogeneous media: Velocity stress finite-difference method. *Geophysics*, 51:889–901, 1986.
[34] K. Willcox and J. Peraire. Balanced model reduction via the proper orthogonal decomposition. *AIAA J.*, 40(11):1–8, 2002.

Department of Computational and Applied Mathematics, Rice University, 6100 Main St., Houston, TX, 77025
*E-mail*: vdovina@rice.edu

Department of Mathematics and Statistics, University of Maryland Baltimore County, 1000 Hilltop Circle, Baltimore, MD, 21250
*E-mail*: sminkoff@math.umbc.edu
*URL*: http://www.math.umbc.edu/∼sminkoff